Building and Environment 48 (2012) 206–214

Contents lists available at SciVerse ScienceDirect

Building and Environment

journal homepage: www.elsevier.com/locate/buildenv

Using RANS turbulence models and Lagrangian approach to predict particle deposition in turbulent channel flows

Naiping Gao[a,*], Jianlei Niu[b], Qibin He[a,*], Tong Zhu[a], Jiazheng Wu[a]

[a] Institute of Refrigeration and Thermal Engineering, School of Mechanical Engineering, Tongji University, 1239# Siping Road, Shanghai, China
[b] Department of Building Services Engineering, The Hong Kong Polytechnic University, Hung Hom, Kowloon, Hong Kong

ARTICLE INFO

Article history:
Received 13 May 2011
Received in revised form
1 August 2011
Accepted 3 September 2011

Keywords:
RANS turbulence models
Discrete random walk model
Particle deposition
Near-wall correction

ABSTRACT

This study investigates the capability and accuracy of three Reynolds-Averaged Navier–Stokes (RANS) turbulence models, i.e. a Reynolds stress model (RSM), a RNG k-ε model, and an SST k-ω model in the prediction of particle deposition in vertical and horizontal turbulent channel flows. The particle movement was simulated using a Lagrangian-based discrete random walk (DRW) model. The performances of the three RANS turbulence models with and without near-wall turbulence corrections were evaluated. A new modification method for turbulence kinetic energy was proposed for the RNG k-ε model and the SST k-ω model. The results were compared with previous experimental data, empirical equation as well as simulation outcomes. It is found that the isotropic SST k-ω model and the RSM model can successfully predict the transition from the diffusion region to the inertia-moderated region. The RNG k-ε model with near-wall modifications can also reflect the V-shape deposition curve although without modifications it greatly over-predicts the deposition velocity and shows an almost straight deposition line. For all of the three turbulence models, application of near-wall corrections is able to improve the simulation results to different extents.

1. Introduction

The study of micro- and nano-meter particle deposition from a turbulent flow onto the adjacent walls has attracted much attention in the past decades due to its wide applications in industry, such as nuclear reactor, air cleaning, fouling/erosion of turbine blades, and air pollution control etc. Since particulate matter is one of the main pollution sources indoors, understanding particle deposition behaviors in ventilation ducts and enclosed environment is also crucial for indoor air quality (IAQ) control. Besides experimental studies and empirical models, computational fluid dynamics (CFD) methods, particularly the Eulerian-Lagrangian methods, are widely used. In these methods, turbulent flow field is treated as a continuous phase and simulated in the Eulerian frame, and discrete particles interact with the flow eddies in the Lagrangian frame.

Generally, direct numerical simulation (DNS), large eddy simulation (LES), and Reynolds-Averaged Navier–Stokes (RANS) simulation are the three approaches to deal with the turbulent flows. For particle–eddy interactions, discrete random walk (DRW) model and continuous filter white-noise (CFWN) model are adopted. Ounis et al. [1] and Zhang and Ahmadi [2] used DNS and DRW model to study particle dispersion and deposition in turbulent channel flows. Beghein et al. [3] used LES and DRW model to study particle transport in a ventilated chamber. Wang and James [4], Matida et al. [5], and Zhang and Chen [6] adopted RANS turbulence models and DRW model to investigate particle dispersion and deposition in turbulent ducts or human respiratory tracts. He and Ahmadi [7] and Mehel et al. [8] adopted a RANS turbulence model and CFWN model to study particle movements in turbulent flows.

Since DNS and LES methods are still far from practical engineering use at present due to their excessive requirement in computing resources, the various RANS turbulence models are the most popular method for turbulent flow simulations although their accuracy and applicability are still issues of debate. Consequently predictions of the fates of particles based on the flow field obtained from RANS models have been tried by many researchers. Tian and Ahmadi [9] compared the standard k-ε model with a Reynolds stress model (RSM) in the Lagrangian frame using both DRW and CFWN approaches. Parker et al. [10] compared particle deposition velocity predicted by a RNG k-ε model, an SST k-ω model, and a RSM model with the experimental data by Liu and

* Corresponding authors. Tel.: +86 21 65983867.
E-mail addresses: gaonaiping@tongji.edu.cn, gaonaiping@gmail.com (N. Gao), heqibin13@hotmail.com (Q. He).

0360-1323/$ – see front matter © 2011 Elsevier Ltd. All rights reserved.
doi:10.1016/j.buildenv.2011.09.003

Agarwal [11]. However, there is still a lack of full comparison of the relative performances of the commonly used RANS turbulence models.

In electrical neutral and isothermal turbulent flows, the main mechanisms responsible for the deposition of micro- and nanometer particles are Brownian diffusion, turbulent diffusion, gravitational settling, shear-induced force, and inertial impaction. As we know, the RANS turbulence models, especially the two-equation models, would exaggerate the turbulent diffusion effect and result in over-prediction of particle deposition velocity for small particles. Previous studies have proposed correction methods to overcome this problem [4,9,12,13]. However, these methods either need a supplementary software package or are not fully verified with good experimental data. It is necessary to carry out further studies on the effect of existing correction methods and to develop a new easy-to-use method which can be easily implemented into CFD-packages.

In this paper, three commonly used RANS turbulence models, i.e. a RNG k-ε model by Yakhot and Orszag [14], an SST k-ω model by Menter [15], and a RSM model by Gibson and Launder [16] combined with the DRW model were adopted to predict particle deposition in vertical and horizontal turbulent channel flows with the aid of the Fluent CFD package [17]. The performances of the three RANS turbulence models with and without near-wall corrections proposed by Matida et al. [12] and Tian and Ahmadi [9] were tested. The experimental data of Liu and Agarwal [11], Sippola and Nazaroff [18], Montgomery and Corn [19], Lai et al. [20], the empirical equation from Wood [21], as well as the simulation results of Tian and Ahmadi [9] were used for comparison. A new correction method was proposed in this study.

2. Numerical method

2.1. Mean flow field

An accurate prediction of airflow pattern is the prerequisite for reliable particle movement modeling. The turbulence model should correctly capture both the mean flow field and the turbulence properties such as turbulence kinetic energy and its dissipation rate. Considering their wide applications in predicting mean flows [4,5,9,10,12], a RNG k-ε model by Yakhot and Orszag [14], an SST k-ω model by Menter [15], and a RSM model by Gibson and Launder [16] were selected in this study. The main differences among these three RANS turbulence models are the strategies to model the time-averaged products of the two fluctuating velocity components, which are called Reynolds stress components $-\overline{\rho u'v'}$. The RSM model, which is not based on the isotropic eddy-viscosity hypothesis, closes the Reynolds-Averaged Navier–Stokes equations by solving six additional transport equations and modeling the time-averaged product of three fluctuating velocity components $\overline{u'v'w'}$. With an equation for the dissipation rate, there are totally five additional transport equations for two-dimensional problems and seven for three-dimensional problems in the second-moment RSM model.

The RNG k-ε model uses transport equations for the turbulence kinetic energy (k) and its dissipation rate (ε) to model the Reynolds stress component, while the SST k-ω model adopts the turbulence kinetic energy (k) and specified dissipation rate (ω) based on the concept of turbulent viscosity. Furthermore, the SST k-ω model uses a blending function to automatically switch between near-wall-region turbulence model and core-region turbulence model. In the near-wall region, it adopts the standard k-ω model while in the core region it applies a transformed k-ε model [15]. The RNG k-ε model and RSM model adopt either wall functions or near-wall models to consider the wall effects on turbulence.

2.2. Particle movements

Lagrangian tracking method calculates individual particle trajectory by solving the particle momentum equation. By equating particle inertia with external forces, the momentum equation in the Cartesian coordinate system can be expressed as [9]:

$$\frac{du_P}{dt} = \frac{1}{\tau}\frac{C_D \mathrm{Re}_P}{24}(u - u_P) + \frac{g(\rho_P - \rho)}{\rho_P} + F_a \tag{1}$$

In Eq. (1), the left-hand side represents the inertial force per unit mass (m/s^2). The first term on the right-hand side is the drag force and the second term the gravity and buoyancy. τ is the particle relaxation time given by Eq. (2). C_D is the drag coefficient given by Eq. (4) and Eq. (5) [22] and Re_P is the particle Reynolds number defined by $\mathrm{Re}_P = d_P|u - u_P|/\nu$.

$$\tau = \frac{S d_P^2 C_c}{18\nu} \tag{2}$$

C_c is the Cunningham slip correction factor that can be computed from [23]:

$$C_c = 1 + \frac{2\lambda}{d_P}\left(1.257 + 0.4e^{-(1.1 d_P/2\lambda)}\right) \tag{3}$$

$$C_D = \frac{24}{\mathrm{Re}_P} \quad \text{for} \quad \mathrm{Re}_P < 1, \tag{4}$$

and

$$C_D = \frac{24}{\mathrm{Re}_P}\left(1 + 0.15\mathrm{Re}_P^{0.687}\right) \quad \text{for} \quad 1 < \mathrm{Re}_P < 400. \tag{5}$$

For the current study, since isothermal condition is assumed, thermophoretic force which is caused by temperature gradients is not taken into account. The additional forces F_a then can be expressed by the sum of Brownian force F_B [24] and Saffman's lift force F_S [25]. That means $F_a = F_B + F_S$. The Brownian force F_B is given by:

$$F_B = \zeta\sqrt{\frac{\pi S_0}{\Delta t}} \tag{6}$$

S_0 is the spectral intensity given by:

$$S_0 = \frac{216\rho\nu k_b T}{\pi\rho_P^2 d_P^5 C_c} \tag{7}$$

The Saffman's lift force F_S is determined by:

$$F_S = \frac{2\rho K_c \nu^{0.5}}{\rho_P d_P (s_{lk} s_{kl})} s_{ij}(u - u_P) \tag{8}$$

where $K_c = 2.594$.

In Eq. (1), instantaneous air velocity could be expressed as $u = \overline{u} + u'$. Mean air flow velocity $\overline{u}$ is predicted by the RANS turbulence models and the way of generating fluctuating velocity u' will be discussed in the next section.

2.3. Discrete random walk (DRW) model

A discrete random walk (DRW) model or so-called eddy-interaction model (EIM) [26] is used to predict the movement of particles caused by turbulent diffusion in channel flows. This model allows one particle to interact successively with various eddies by giving its initial conditions of velocity and location. Each eddy has a characteristic lifetime, length scale, and velocity scale. The

interaction between a particle and an eddy ends when the lifetime of the eddy is over or when the particle crosses the eddy boundary. At that time, a new interaction between the particle and a new eddy starts [5].

The particle Lagrangian integral time scale τ_L for the two-equation RANS turbulence models (the RNG k-ε and SST k-ω models here) can be expressed as:

$$\tau_L = C_1\frac{k}{\varepsilon} \tag{9}$$

The value of C_1 is obtained according to experimental data. There is no a universal value. In this study, $C_1 = 0.32$ suggested by Hinze [27] was used.

For the RSM model, τ_L can be expressed as:

$$\tau_L = C_2\frac{(v'_{\mathrm{rms}})^2}{2\varepsilon} \cong C_3\frac{k}{\varepsilon} \tag{10}$$

v'_{rms} is the local root-mean-square (RMS) value of the velocity fluctuations ($(v'_{\mathrm{rms}} = \sqrt{\overline{v'^2}})$) and $C_3 = 0.3$ here.

The characteristic lifetime of the eddy is calculated as follows [17]:

$$\tau_e = -\tau_L \log(r) \tag{11}$$

Here r is a uniform random number between 0 and 1. Random calculation of τ_e rather than using a constant $\tau_e(=2\tau_L)$ gives better results [17].

The particle crossing time τ_{cross} is defined as:

$$\tau_{\mathrm{cross}} = -\tau \ln\left[1 - \left(\frac{L_e}{\tau|u-u_P|}\right)\right] \tag{12}$$

where τ is the particle relaxation time defined by Eq. (2), $L_e = (C_\mu)^{3/4}(k^{3/2}/\varepsilon)$ is the eddy length scale, and $|u-u_P|$ is the magnitude of the relative slip velocity.

The DRW model assumes that fluctuating velocities follow a Gaussian probability distribution. The fluctuating velocity component u' has the following form:

$$u' = \zeta u'_{\mathrm{rms}} \tag{13}$$

For the RNG k-ε model and SST k-ω model, the values of the RMS fluctuating components can be defined as:

$$u'_{\mathrm{rms}} = v'_{\mathrm{rms}} = w'_{\mathrm{rms}} = \sqrt{2k/3} \tag{14}$$

Here turbulent fluctuations are assumed to be isotropic.

For the RSM model, anisotropy of the stresses is included in the derivation of the velocity fluctuations:

$$u' = \zeta u'_{\mathrm{rms}} \tag{15}$$

$$v' = \zeta v'_{\mathrm{rms}} \tag{16}$$

$$w' = \zeta w'_{\mathrm{rms}} \tag{17}$$

3. Corrections of turbulent fluctuating velocities in the near-wall region

3.1. Corrections for the Reynolds stress model

Previous studies have shown that an accurate simulation of near-wall anisotropic turbulent fluctuations is crucial for predicting deposition of small particles with the EIM model [4,12]. From Eqs. (15)–(17), we can observe that the RSM model could account for the anisotropic feature of the instantaneous fluctuating velocities in three directions. This study also evaluated two sets of curve-fitted RMS values of the fluctuating velocities from DNS used by Matida et al. [12] and Tian and Ahmadi [9].

Matida et al. [12] adopted the RMS values of the fluctuating velocities from a DNS simulation of two-dimensional channel flows [28]. The expressions of the three RMS values normalized by the friction velocity u^* are as follows:

$$\frac{u'_{\mathrm{rms}}}{u^*} = \frac{0.40y^+}{1+0.0239(y^+)^{1.496}} \tag{18}$$

$$\frac{v'_{\mathrm{rms}}}{u^*} = \frac{0.0116(y^+)^2}{1+0.203y^+ + 0.00140(y^+)^{2.421}} \tag{19}$$

$$\frac{w'_{\mathrm{rms}}}{u^*} = \frac{0.19y^+}{1+0.0361(y^+)^{1.322}} \tag{20}$$

In this study, Eqs. (18)–(20) were applied in the region $y^+ < 30$.

Tian and Ahmadi [9] pointed out that only the fluctuating velocity normal to the wall was important to the calculation of the particle deposition velocity. They adopted a simple quadratic variation expression of v'_{rms} versus y^+ in the region of $y^+ < 4$ based on the data by Kim et al. [29]:

$$\frac{v'_{\mathrm{rms}}}{u^*} = C\left(y^+\right)^2 \tag{21}$$

Here C is a constant and it was suggested to be 0.008 by Ounis et al. [1].

3.2. Corrections for the two-equation models

Typically, there are two types of near-wall corrections for the two-equation turbulence models in the literature. The first type is to keep the mean flow properties from the two-equation turbulence models meanwhile introduce the RMS values of the velocity fluctuations from curve-fitted DNS values in three directions or only in the direction normal to the wall [4,9]. In order to implement this type of method, one should either import the mean flow information into a separate particle calculation code or switch the two-equation turbulence models to the RSM model in the CFD package since the two-equation turbulence models can not directly solve the RMS values.

The second type is to reduce the near-wall turbulence kinetic energy [5,13]. It still assumes the isotropic fluctuations in the boundary layer. But the turbulence kinetic energy is artificially reduced as follows [13]:

$$\frac{u'_{\mathrm{rms}}}{u^*} = \frac{v'_{\mathrm{rms}}}{u^*} = \frac{w'_{\mathrm{rms}}}{u^*} = C\left(y^+\right)^2 \tag{22}$$

$$k = \frac{(u'_{\mathrm{rms}})^2+(v'_{\mathrm{rms}})^2+(w'_{\mathrm{rms}})^2}{2} = \frac{3(v'_{\mathrm{rms}})^2}{2} = \frac{3\left(Cu^*(y^+)^2\right)^2}{2} \tag{23}$$

Here C equals 0.008 [1]. Lai and Chen [13] used Eqs. (22) and (23) in the region $y^+ < 4$.

We used the RNG k-ε model and Eq. (23) to test the second type of method in vertical channel flows. During the calculation process, it was found that this method would result in under-prediction of the particle deposition velocity and required a very long calculation time. For example, it showed no deposition of 1 μm particles even

when 100,000 trajectories were released. The shortcoming of this method might be that it under-estimates the near-wall turbulence kinetic energy too much.

To improve the correction method by Matida et al. [5] and Lai and Chen [13], a simplified correction for near-wall turbulence kinetic energy was proposed by introducing an empirical correction factor C_k. The RMS of fluctuations can be expressed by using simple relationships in the near-wall region as follows [12]:

$$\frac{u'_{\mathrm{rms}}}{u^*} \approx 0.4y^+ \tag{24}$$

$$\frac{v'_{\mathrm{rms}}}{u^*} \approx 0.008\left(y^+\right)^2 \tag{25}$$

$$\frac{w'_{\mathrm{rms}}}{u^*} \approx 0.19y^+ \tag{26}$$

The corrected turbulence kinetic energy in the region of $y^+ < 4$ can be expressed by:

$$k = C_k \frac{(0.4u^*y^+)^2 + \left(\left(0.008u^*\left(y^+\right)^2\right)^2 + (0.19u^*y^+)^2\right.}{2} \tag{27}$$

Here C_k is an empirical correction factor smaller than 1.0. Based on a number of tests, we suggest that C_k be in the range of 0.05–0.15.

4. Calculation method for the particle deposition velocity

It is common to present the non-dimensional deposition velocity versus the non-dimensional particle relaxation time [30]. The non-dimensional particle deposition velocity is given by [9]:

$$u_d^+ = \frac{J}{C_0 u^*} \tag{28}$$

The non-dimensional particle relaxation time is computed by [9]:

$$\tau^+ = \frac{\tau(u^*)^2}{\nu} = \frac{Sd_P^2(u^*)^2 C_c}{18\nu^2} \tag{29}$$

The method developed by Kallio and Reeks [31] and Matida et al. [12] was used to calculate the non-dimensional particle deposition velocity:

$$u_d^+ = \frac{\overline{U}A}{u^*P\Delta x}\ln\left(\frac{N_{\mathrm{in}}}{N_{\mathrm{out}}}\right) \tag{30}$$

5. Case description

Two-dimensional turbulent particle-laden channel airflows were simulated. The channel is 0.02 m in width and 0.4 m in length. Structured grids are used to discretize the computational domain in which the first grids are 0.05 mm away from the wall. The y^+ value for the first grid points was about 1.13. The cells evolve to the core region with a growth factor of 1.2. In the core region, the cell size is 0.5 mm × 0.5 mm. The horizontal or vertical channel flow is identified by setting gravitational acceleration along lateral or stream-wise directions. The air properties are: $T = 288$ K, kinematic viscosity $\nu = 1.502 \times 10^{-5}$ m^2/s, and density $\rho = 1.225$ kg/m^3. The Reynolds number based on the mean flow velocity and channel width is 6658.

A fully developed velocity profile with the 1/7th power law in channel flow, turbulence kinetic energy k, and its dissipation rate ε (or specified dissipation rate ω) were set at the inlet boundary by Eq. (31) to Eq. (34):

$$u = \frac{8}{7}U_{\mathrm{mean}}\left(\frac{H}{h/2}\right)^{1/7} \tag{31}$$

where $U_{\mathrm{mean}} = 5.0$ m/s is the average velocity at the cross-section and $H = y$ for $0 \le y \le h/2$ or $H = h - y$ for $h/2 < y \le h$.

$$k = \frac{\tau_w}{\rho\sqrt{C_\mu}} + \frac{H}{h/2}\left\{0.002\left[\frac{8}{7}U_{\mathrm{mean}}\right]^2 - \frac{\tau_w}{\rho\sqrt{C_\mu}}\right\} \tag{32}$$

$$\varepsilon = \frac{C_\mu^{3/4}k^{3/2}}{\kappa y} \tag{33}$$

$$\omega = \frac{k^{1/2}}{C_\mu^{1/4}\kappa y} \tag{34}$$

At the outlet, the Neumann boundary condition was applied for velocity. The walls were adiabatic and there was no slip of air at the walls. The two-layer enhanced wall treatment was applied for the RNG k-ε model and RSM model. For the SST k-ω model, a one-equation low-Reynolds model would automatically be activated depending on the near-wall grid density.

Due to the small particle sizes and low concentration level in this study, the interaction between the air and the particles is treated as one-way coupling, assuming that the effect of particles on the turbulent flow is negligible. Particle sizes were in the range of 0.01 μm–50 μm and the particle-to-fluid density ratio was set as $S = \rho_P/\rho = 2000$. Particles were released into the channel from 100 equispaced locations over the range of $0 < y^+ < 30$ (the bottom wall for the horizontal channel) at the midsection of the channel. The initial streamwise velocity of particles was equal to the local air velocity. The normal velocity was set to zero. A stick wall condition was imposed, i.e., no particle rebounded or resuspended in the calculation. Given the fact that the differences among the particle deposition velocities in this study were of five to six orders of magnitude, 16,000 to 8,000,000 particle trajectories were calculated for each particle size to ensure the stability of the statistical significance.

The governing equations for the continuous phase were converted into algebraic equations by the finite volume method. The convection and diffusion terms were discretized by second-order upwind scheme and second-order central difference scheme, respectively. The SIMPLE algorithm was adopted to couple the pressure and velocity calculations. The differential equation of particle movement was solved based on the Runge-Kutta scheme. The corrections of the fluctuating velocities were implemented into the commercial code through a user-written sub-program.

6. Results and discussions

6.1. The vertical channel condition

The results of the particle deposition velocity in a vertical down stream channel flow (gravity is in the same direction of the main flow) are presented in this section. Fig. 1 shows that the non-dimensional particle deposition velocity presents a V-shape curve and falls into three distinct categories. They are diffusion regime, diffusion-impaction regime, and inertia-moderated regime [30]. In the diffusion regime, particle deposition is mainly affected by the combination of Brownian and turbulent diffusion. The particle

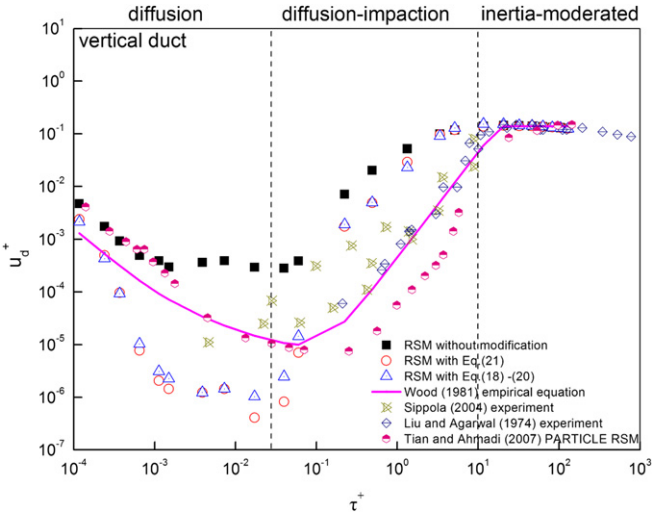

Fig. 1. Comparison of the particle deposition velocities from the RSM model with earlier results in a vertical channel.

deposition velocity decreases as τ^+ increases. In the inertia-moderated regime, large-scale eddy motions would carry particles into the concentration boundary layer and make particles deposit onto the wall due to their large inertia. There is a slight decrease of the particle deposition velocity for coarse particles. The process of particle deposition in the diffusion-impaction regime is affected by turbulent diffusion, inertia-impaction, as well as shear-induced lift force. The particle deposition velocity could increase by three to four orders of magnitude in this region.

The RSM model without near-wall corrections could reflect the distinction of the three deposition regimes. But, the predicted deposition velocity only increases two to three orders of magnitude in the diffusion-impaction regime. The predicted deposition velocity agrees well with the empirical equation and experimental data at the beginning of the diffusion regime and in the inertia-moderated regime. It over-predicts the deposition velocity in the diffusion-impaction regime.

It is found that the deposition velocities from the models with near-wall corrections are smaller in the diffusion and diffusion-impaction regime. It could be ascribed to the smaller value of normal velocity fluctuation in $y^+ < 4$ (as seen from Fig. 2), which leads to a weaker turbulent diffusion impact. It is also observed that near-wall corrections mainly affect the results in $\tau^+ = 10^{-3} - 10^{-1}$, indicating that the effect of turbulent diffusion on particle deposition is essential in this region. The effect of adopting Eq. (21) alone is nearly identical to that of Eqs. (18)–(20), which proves the previous findings that velocity fluctuation normal to the wall in the near-wall region ($y^+ < 4$) is crucial for particle deposition calculation.

Fig. 2 demonstrates the non-dimensional RMS values of turbulent velocity fluctuations in the middle section of the channel flow perpendicular to the wall. In general, the prediction from the RSM model agrees with the DNS results of Eqs. (18)–(20) except that v'^+ is higher in the region of $y^+ < 4$. Eq. (19) and Eq. (21) almost give the same value of v'^+ in $y^+ < 3.0$.

Fig. 3 shows the particle deposition velocities predicted by the RNG k-ε model. The simulation result of Tian and Ahmadi [9] in Fig. 3 is from the standard k-ε model combined with CFWN model using Eq. (21) for the near-wall correction. It is observed that the RNG k-ε model without modifications couldn't tell the differences of the three regimes and greatly over-predicts the particle deposition velocity (one to three orders of magnitude) in the diffusion and diffusion-impaction regimes. This is mainly due to the isotropic

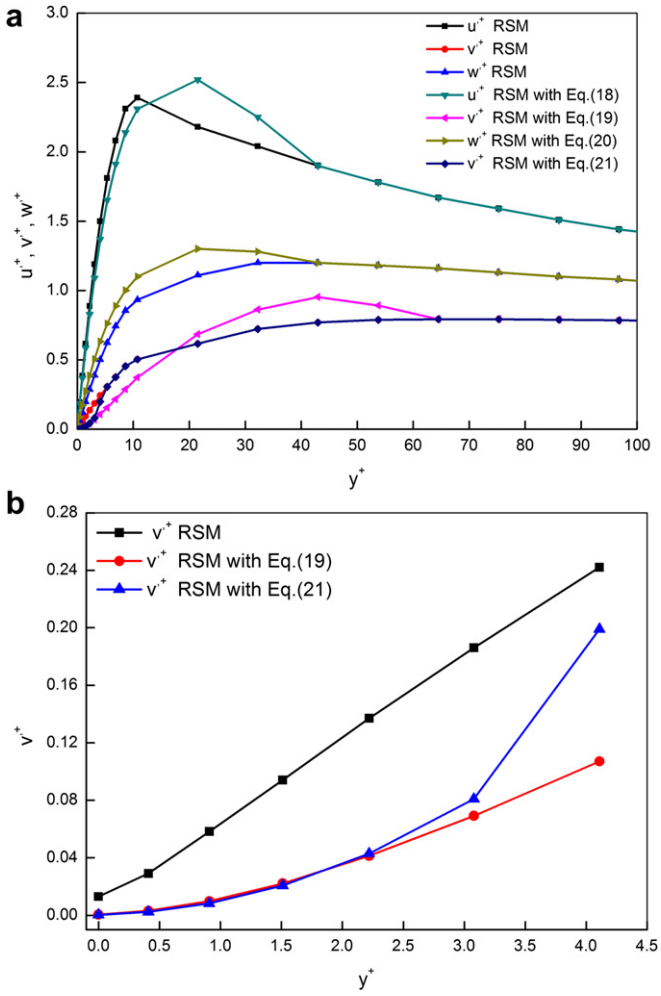

Fig. 2. The non-dimensional root-mean-square (RMS) values of the velocity fluctuations in the middle section of the channel flow perpendicular to the wall (a: three components in $y^+<100$; b: velocity fluctuation normal to the wall in $y^+<4$).

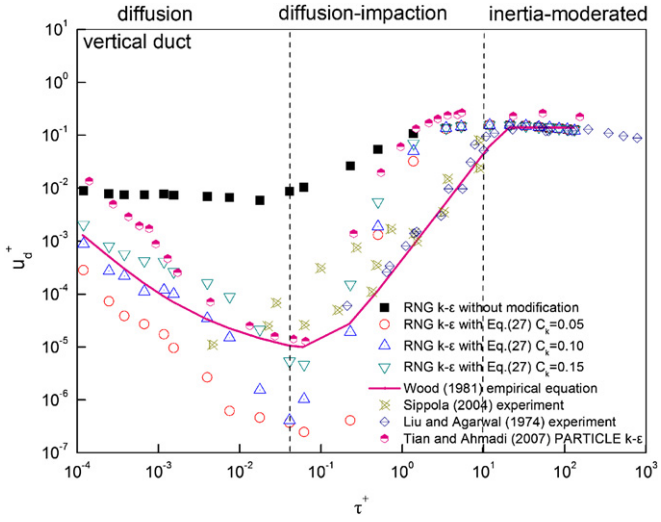

Fig. 3. Comparison of the particle deposition velocities from the RNG k-ε model with earlier results in a vertical channel.

decomposition of turbulence kinetic energy which remarkably exaggerates the normal velocity fluctuation.

When using the near-wall correction of Eq. (27), the results are significantly improved. In the diffusion regime, the results of $C_k = 0.10$ precisely meet the empirical equation. The results of $C_k = 0.15$ are slighter higher and the results of $C_k = 0.05$ are slightly lower. The smaller the value of C_k, the lower the particle deposition velocity appears. This is because smaller C_k means smaller turbulence kinetic energy, and further smaller turbulent velocity fluctuations and a weaker turbulent diffusion effect. The near-wall correction of Eq. (27) under-predicts the deposition velocity in the valley of the V-shape curve and slightly over-predicts the deposition velocity in the diffusion-impaction regime. Again, near-wall corrections affect the results significantly in $\tau^+ = 10^{-3} - 10^{-1}$. In the inertia-moderated regime, the results with and without near-wall corrections are almost the same and correspond to the experimental data well.

In Fig. 4, the results showed that the isotropic SST k-ω model predicts particle deposition rather well without any near-wall corrections. It seems to conflict with the traditional view that all isotropic two-equation RANS turbulence models with the Lagrangian DRW model would over-predict the deposition velocity of fine particles. It is encouraging that the SST k-ω model itself could predict the deposition velocity with the similar trend in the empirical equations by distinguishing the three regimes. The prediction precision is at least as high as the RSM model.

Fig. 5 demonstrates normalized turbulence kinetic energy profiles in the middle section of the channel flow perpendicular to the wall. Both the RNG k-ε model and SST k-ω model are in line with the DNS results [28], moreover the SST k-ω model meets the DNS results better. Considering the particle deposition results in Figs. 3 and 4, it can be derived that the near-wall turbulence kinetic energy and velocity fluctuation normal to the wall are not the only reason affecting deposition caused by turbulent diffusion. The near-wall turbulence kinetic energy predicted from the SST k-ω model is higher than that from the RNG k-ε model. But the particle deposition velocity predicted by the SST k-ω model is smaller in the diffusion and diffusion-impaction regime.

Without modifications, the SST k-ω model is able to predict a V-shape deposition curve whereas the RNG k-ε model can not although both models give similar turbulence kinetic energy in the boundary layer. This phenomenon reminds us that besides k and the average flow velocity, there are other factors affecting particle deposition. In the eddy-interaction model, the eddy length scale and the Lagrangian integral time scale are calculated differently in the two turbulence models. $L_e = k^{1/2}/C_\mu^{1/4}\omega$ and $\tau_L = C_1/\omega$ for the SST k-ω model. $L_e = C_\mu^{3/4}k^{3/2}/\varepsilon$ and $\tau_L = C_1 k/\varepsilon$ for the RNG k-ε model. Fig. 6 illustrates that the eddy length scales predicted by the RNG k-ε model and the SST k-ω model are very close in $y^+<35$. However, the Lagrangian integral time scale from the SST k-ω model is much lower than that from the RNG k-ε model. A lower integral time scale means more frequent interactions between particles and the turbulent eddies, which may decrease the deposition velocity. This may explain why the RNG k-ε and the SST k-ω model perform differently when τ^+ is between 10^{-2} and 10^{-1}. For a further investigation, C_1 of the RNG k-ε model was artificially reduced to 0.05 and 0.01, the respective deposition velocity for 0.1 μm particles ($\tau^+ = 1.50 \times 10^{-3}$) was only about 72% and 10% of that of $C_1 = 0.32$.

It should be mentioned that smaller integral time and length scale would lead to longer particle calculation time. For instance, for a certain particle size and the same constant C_1, the calculation time for the SST k-ω model is longer than that for the RNG k-ε model. Regarding the RNG k-ε model, the calculation time of $C_1 = 0.01$ is more than 10 times of that of $C_1 = 0.32$.

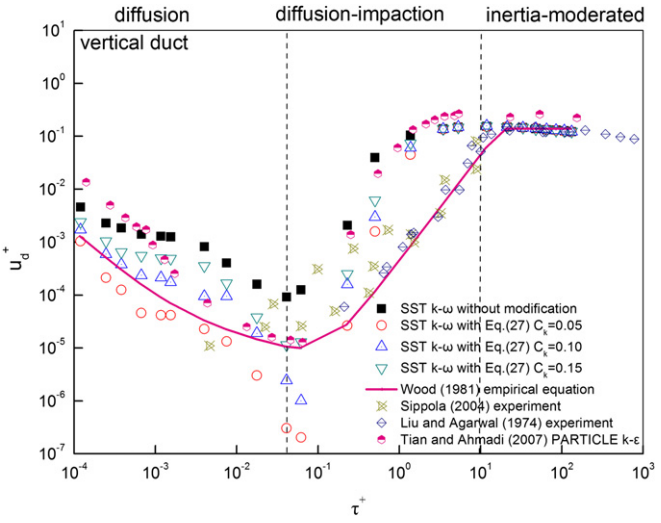

Fig. 4. Comparison of the particle deposition velocities from the SST k-ω model with earlier results in a vertical channel.

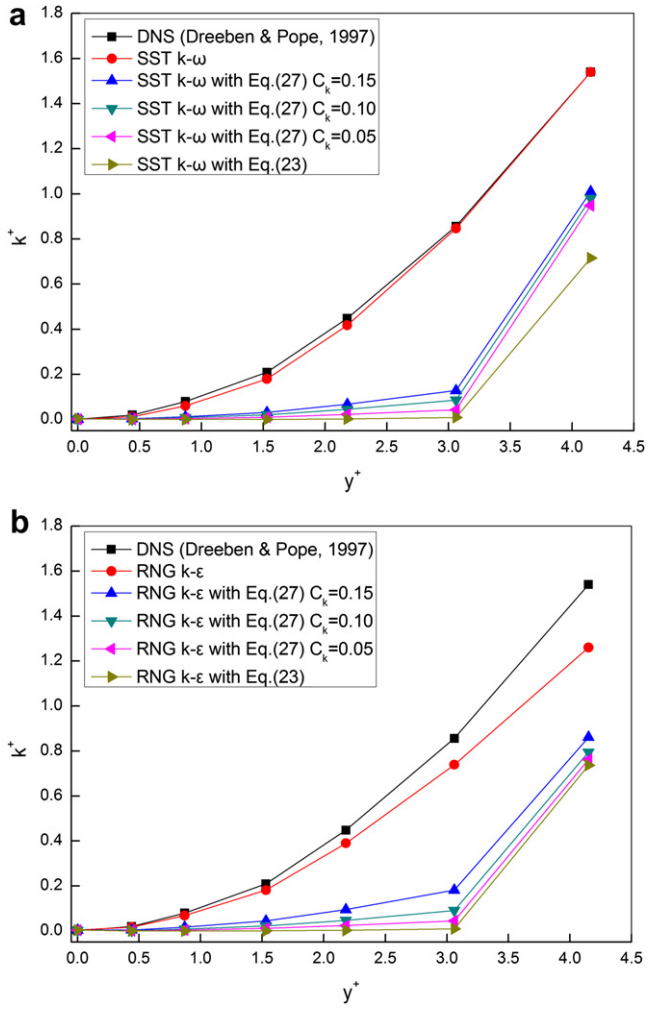

Fig. 5. The normalized turbulence kinetic energy profiles in the near-wall region in the middle section of the channel flow perpendicular to the wall (a: the SST k-ω model; b: the RNG k-ε model).

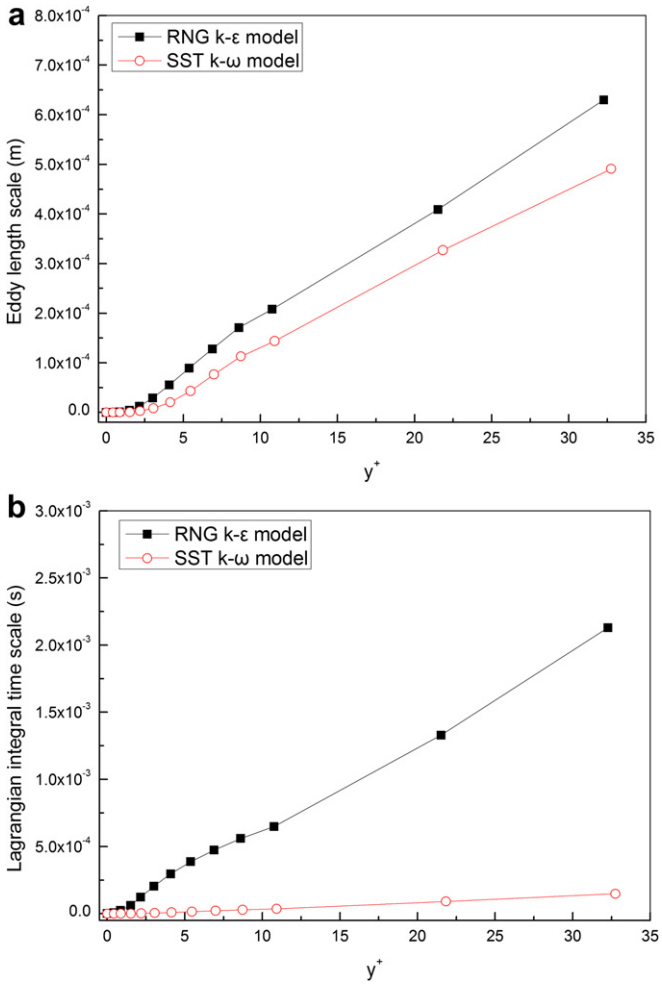

Fig. 6. Eddy length scale (a) and Lagrangian integral time scale (b) predicted by the RNG k-ε and the SST k-ω model.

If using Eq. (27) to correct near-wall turbulence, the predicted results from the SST k-ω model are improved to a certain extent. It indicates that the method of empirical correction factors works well in both the RNG k-ε model and the SST k-ω model. It should be noted that the correction also reduces the Lagrangian integral time scale because of the decreased turbulence kinetic energy, indicating a longer calculation time.

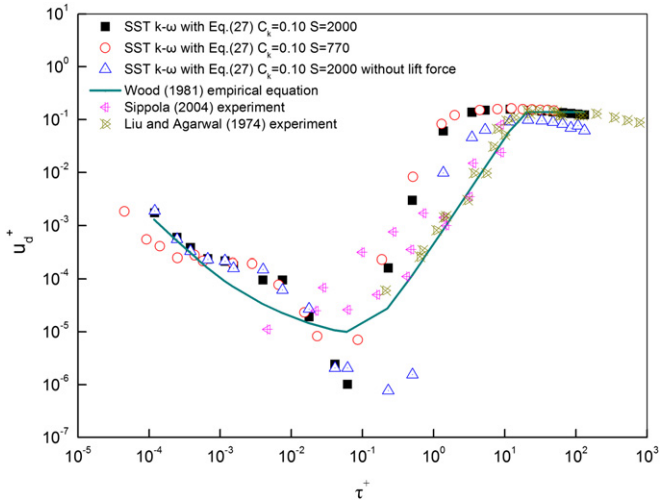

Fig. 7. The particle deposition velocities from the SST k-ω model under various conditions.

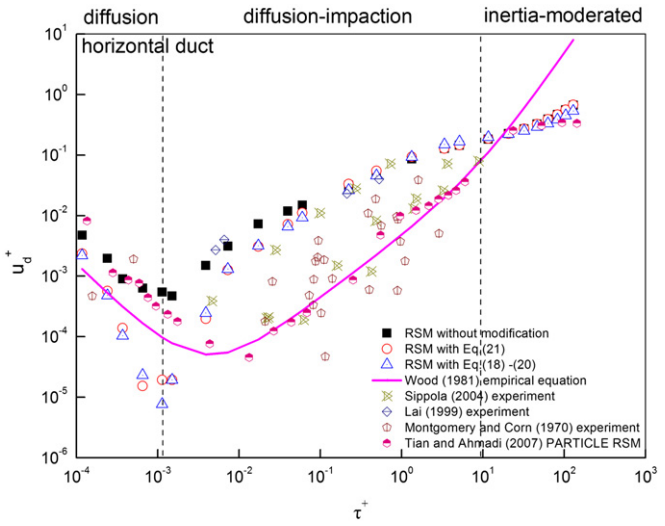

Fig. 8. Comparison of the particle deposition velocities from the RSM model with earlier results in a horizontal channel.

Figs. 1,3,4 all show that the main differences among the simulated results and experimental data are in the valley of the V-shape curve and in the diffusion-impaction regime. To further investigate this issue, we calculated the particle deposition velocity (see Fig. 7) at a particle-to-fluid density ratio of $S = \rho_P/\rho = 770$, which was the same as the experimental condition of Liu and Agarwal [11]. Although presented in the non-dimensional form, the particle-to-fluid density ratio still affects the deposition velocity, especially in the valley of the V-shape curve. The deposition velocities when $S = 770$ correspond to the experimental data and the empirical equation better than when $S = 2000$. Therefore, the non-dimensional deposition velocity is not only determined by the non-dimensional relaxation time but also affected by other factors, such as particle-to-fluid density ratio.

Kallio and Reeks [31] presented that the shear-induced lift force could increase the particle deposition velocity significantly in $1 < \tau^+ < 10$ and they believed that Saffman's [25] expression for the shear-induced lift force should be regarded as approximate within the boundary layer. Fig. 7 examines the effect of exclusion of

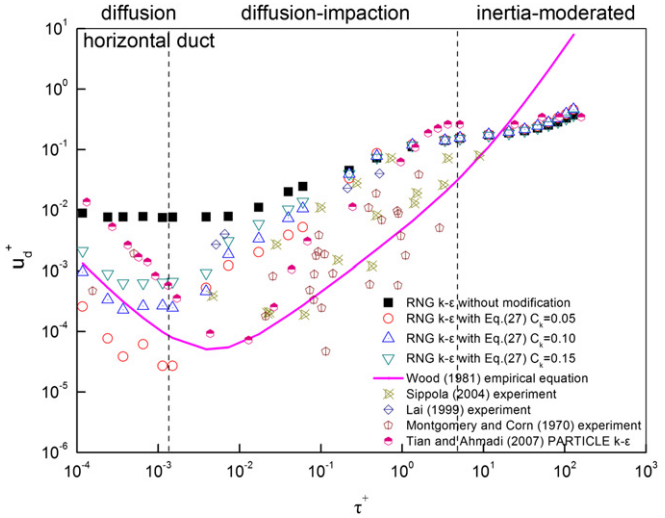

Fig. 9. Comparison of the particle deposition velocities from the RNG k-ε model with earlier results in a horizontal channel.

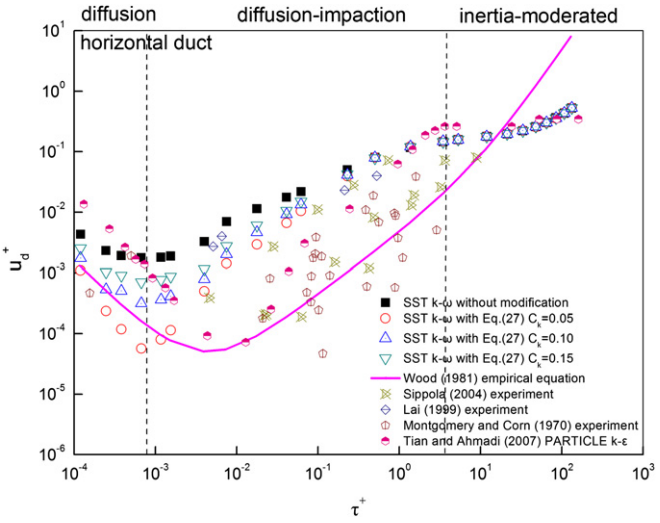

Fig. 10. Comparison of the particle deposition velocities from the SST k-ω model with earlier results in a horizontal channel.

Saffman's lift force when calculating particle deposition. It is found that the result without Saffman's lift force is better in $1 < \tau^+ < 10$. However, in the inertia-moderated regime and in $10^{-1} < \tau^+ < 1$, the simulation without Saffman's lift force under-estimates the particle deposition velocity.

6.2. The horizontal channel condition

Figs. 8–10 illustrate the particle deposition velocities predicted by the RSM model, the RNG k-ε model, and the SST k-ω model, individually. In the horizontal channel, gravity is perpendicular to the flow direction. Therefore it assists the particle deposition. In comparison with the vertical channel, the particle deposition velocity in the horizontal channel also falls into three categories notwithstanding the characteristics in each regime are changed a little. The diffusion regime is narrowed and the diffusion-impaction regime is broadened due to the additional gravity force. In the inertia-moderated regime, the particle deposition velocity always increases with particle size.

In the horizontal channel, the effect of near-wall corrections is not as obvious as in the vertical channel. Inclusion of near-wall corrections only affects deposition of particles in $\tau^+ < 10^{-1}$, suggesting that turbulent diffusion is less essential to particle deposition in horizontal channel flows than in vertical channel flows for $\tau^+ > 10^{-1}$. The most significant improvement when adopting near-wall corrections, by one to two orders of magnitude, appears in the RNG k-ε model. Another finding is that for the two-equation models, the best C_k is 0.05 for the horizontal channel flow and 0.10 for the vertical channel flow. The worst situation still exists in the diffusion-impaction regime, where the deposition velocities are higher than the experimental data and the empirical equation for all of the three turbulence models.

7. Conclusions

The capability and accuracy of three Reynolds-Averaged Navier–Stokes (RANS) turbulence models, i.e. a Reynolds stress model (RSM), a RNG k-ε model, and an SST k-ω model, to predict the particle deposition in vertical and horizontal turbulent channel flows in the frame of Lagrangian approach were investigated. The effects of near-wall corrections proposed by Matida et al. [12] and Tian and Ahmadi [9] for the RSM model as well as a new simple correction method for the two-equation models were evaluated by using previous experimental data and one empirical equation. The main conclusions are as follows:

(1). The anisotropic RSM model itself is able to distinguish the three deposition regimes though it predicts higher deposition velocities than experimental data and the empirical equation in the diffusion and diffusion-impaction regime. Near-wall corrections make the deposition velocity smaller than the empirical equation in the diffusion regime and still slightly higher than experimental data and the empirical equation in the diffusion-impaction regime. The effects of correction methods proposed by Matida et al. [12] and Tian and Ahmadi [9] are nearly the same.

(2). The RNG k-ε model itself can not differentiate the three deposition regimes and greatly over-predicts the deposition velocity in the diffusion and diffusion-impaction regimes. Near-wall corrections could greatly improve its performance.

(3). The isotropic two-equation SST k-ω model predicts the particle deposition velocity as the RSM model does due to its smaller Lagrangian integral time scale (if compared with the RNG k-ε model). When combined with near-wall corrections, the results are improved to some extents.

(4). The near-wall corrections could influence the effect of turbulence diffusion on particle deposition and mainly affect the deposition velocity in the range of $\tau^+ = 10^{-3} - 10^{-1}$.

(5). Even with near-wall corrections, all of the three RANS turbulence models still over-predict the deposition velocity in the diffusion-impaction regime. But in the inertia-moderated regime, they agree with experimental data very well.

Acknowledgment

This study was financially supported by the Research Grant Committee, Hong Kong, China, under the project No. RGC GRF 526508, the National Natural Science Foundation of China under the project No. 50808133, and the Program of Young Excellent Teachers in Tongji University.

References

[1] Ounis H, Ahmadi G, McLaughlin J. Brownian particle deposition in a directly simulated turbulent channel flow. Phys Fluids A-Fluid 1993;5:1427.
[2] Zhang HF, Ahmadi G. Aerosol particle transport and deposition in vertical and horizontal turbulent duct flows. J Fluid Mech 2000;406:55–80.
[3] Beghein C, Jiang Y, Chen QY. Using large eddy simulation to study particle motions in a room. Indoor Air 2005;15:281–90.
[4] Wang Y, James PW. On the effect of anisotropy on the turbulent dispersion and deposition of small particles. Int J Multiphase Flow 1999;25:551–8.
[5] Matida EA, Finlay WH, Lange CF, Grgic B. Improved numerical simulation of aerosol deposition in an idealized mouth-throat. J Aerosol Sci 2004;35:1–19.
[6] Zhang Z, Chen Q. Prediction of particle deposition onto indoor surfaces by CFD with a modified Lagrangian method. Atmos Environ 2009;43:319–28.
[7] He CH, Ahmadi G. Particle deposition in a nearly developed turbulent duct flow with electrophoresis. J Aerosol Sci 1999;30:739–58.
[8] Mehel A, Tanière A, Oesterlé B, Fontaine J- R. The influence of an anisotropic Langevin dispersion model on the prediction of micro- and nanoparticle deposition in wall-bounded turbulent flows. J Aerosol Sci 2010;41:729–44.
[9] Tian L, Ahmadi G. Particle deposition in turbulent duct flows – comparisons of different model predictions. J Aerosol Sci 2007;38:377–97.
[10] Parker S, Foat T, Preston S. Towards quantitative prediction of aerosol deposition from turbulent flows. J Aerosol Sci 2008;39:99–112.
[11] Liu B, Agarwal J. Experimental observation of aerosol deposition in turbulent flow. J Aerosol Sci 1974;5:145–8.
[12] Matida EA, Nishino K, Torii K. Statistical simulation of particle deposition on the wall from turbulent dispersed pipe flow. Int J Heat and Fluid Flow 2000; 21:389–402.
[13] Lai ACK, Chen FZ. Modeling particle deposition and distribution in a chamber with a two-equation Reynolds-averaged Navier–Stokes model. J Aerosol Sci 2006;37:1770–80.
[14] Yakhot V, Orszag S. Renormalization group analysis of turbulence. I. Basic theory. J Scientific Computing 1986;1:3–51.

[15] Menter F. Two-equation eddy-viscosity turbulence models for engineering applications. AIAA Journal 1994;32:1598–605.
[16] Gibson MM, Launder BE. Ground effects on pressure-fluctuations in atmospheric boundary-layer. J Fluid Mech 1978;86:491–511.
[17] Fluent. Fluent 6.3 user's guide. Lebanon: NH 03766, USA; 2006.
[18] Sippola MR, Nazaroff WW. Experiments measuring particle deposition from fully developed turbulent flow in ventilation ducts. Aerosol Sci Technol 2004; 38:914–25.
[19] Montgomery TL, Corn M. Aerosol deposition in a pipe with turbulent airflow. J Aerosol Sci 1970;1:185–94. IN3, 95-213.
[20] Lai ACK, Byrne MA, Goddard AJH. Measured deposition of aerosol particles on a two-dimensional ribbed surface in a turbulent duct flow. J Aerosol Sci 1999; 30:1201–14.
[21] Wood NB. A simple method for the calculation of turbulent deposition to smooth and rough surfaces. J Aerosol Sci 1981;12:275–90.
[22] Hinds WC. Aerosol technology: properties, behavior, and measurement of airborne particles. 2nd ed. New York: A Wiley-Interscience Publication; 1998.
[23] Ounis H, Ahmadi G. Analysis of dispersion of small spherical particles in a random velocity field. J Fluids Eng 1990;112:114–20.
[24] Li A, Ahmadi G. Dispersion and deposition of spherical-particles from point sources in a turbulent channel flow. Aerosol Sci Technol 1992;16:209–26.
[25] Saffman PG. Lift on a small sphere in a slow shear flow. J Fluid Mech 1965;22: 385–400.
[26] Graham DI, James PW. Turbulent dispersion of particles using eddy interaction models. Int J Multiphase Flow 1996;22:157–75.
[27] Hinze J. Turbulence. 2nd ed. New York: McGraw-Hiil; 1975.
[28] Dreeben T, Pope S. Probability density function and Reynolds-stress modeling of near-wall turbulent flows. Phys Fluids 1997;9:154–63.
[29] Kim J, Moin P, Moser R. Turbulence statistics in fully developed channel flow at low Reynolds number. J Fluid Mech 1987;177:133–66.
[30] Guha A. Transport and deposition of particles in turbulent and laminar flow. Annu Rev Fluid Mech 2008;40:311–41.
[31] Kallio GA, Reeks MW. A numerical simulation of particle deposition in turbulent boundary layers. Int J Multiphase Flow 1989;15:433–46.

Glossary

A: cross-sectional area of the boundary layer in Eq.(30)
C, C_1, C_2, $C_3 = 0.3$: model constant
C_0: particle concentration
C_c: Cunningham correction to Stokes' drag law
C_D: drag coefficient
C_k: empirical correction factor
C_μ: empirical constant, equal to 0.09
d_P: particle diameter
F_a: additional forces per unit mass
F_B: Brownian force
F_S: Saffman's lift force
g: gravitational acceleration vector
J: particle mass flux to the wall per unit time
k: turbulence kinetic energy
k^+: normalized turbulence kinetic energy, $k^+ = k/(u^*)^2$
k_b: Boltzmann constant
K_c: model constant
L_e: eddy length scale
$N_{in}N_{out}$: total number of particles entering and exiting the boundary layer
P: perimeter
r: uniform random number between 0 and 1
Re_P: particle Reynolds number
S: particle-to-fluid density ratio
S_0: spectral intensity
s_{ij}: components of the mean strain tensor
t: time
Δt: time step in the particle calculation
T: absolute temperature
u: air velocity
$\overline{U}$: average streamwise fluid velocity across the boundary layer in Eq.(30)
U_{mean}: average velocity of the cross section
u', v', w': fluctuating velocity components
$u'_{rms}, v'_{rms}, w'_{rms}$: root-mean-square of fluctuating velocity components
u'^+, v'^+, w'^+: non-dimensional root-mean-square of fluctuating velocity components $u'^+ = u'_{\mathrm{rms}}/u^*$, $v'^+ = v'_{\mathrm{rms}}/u^*$, $w'^+ = w'_{\mathrm{rms}}/u^*$
u^*: wall friction velocity
u_d^+: non-dimensional particle deposition velocity
$\overline{u}$: mean air velocity
u_P: particle velocity
Δx: incremental length of the, equal to 0.2 m in this study
y: distance normal to the wall
y^+: dimensionless distance normal to the wall, $y^+ = yu^*/\nu$

Greek symbols
ε: turbulence kinetic energy dissipation rate
ζ: normally distributed random number
κ: von Karman constant
λ: gas molecular mean free path$\lambda = 0.066$ μm
ν: kinematic viscosity
ρ: air density
ρ_P: particle density
τ: particle relaxation time
τ_{cross}: particle crossing time
τ_e: characteristic lifetime of the eddy
τ_L: particle Lagrangian integral time scale
τ_w: wall shear stress of the fluid
ω: specified dissipation rate